Kinetic Monte Carlo model for the COVID-19 epidemic: Impact of mobility restriction on a COVID-19 outbreak

Leonardo Evaristo de Sousa

Theoretical and Structural Chemistry Group, State University of Goias, 75132-400, Anapolis, Brazil

Pedro Henrique de Oliveira Neto and Demetrio Antônio da Silva Filho [*]

Institute of Physics, University of Brasilia, 70919-970, Brasilia, Brazil

As the coronavirus disease 2019 (COVID-19) spreads worldwide, epidemiological models have been employed to evaluate possible scenarios and gauge the efficacy of proposed interventions. Considering the complexity of disease transmission dynamics in cities, stochastic epidemic models include uncertainty in their treatment of the problem, allowing the estimation of the probability of an outbreak, the distribution of epidemic magnitudes, and their expected duration. In this sense, we propose a kinetic Monte Carlo epidemic model that focuses on demography and on age-structured mobility data to simulate the evolution of the COVID-19 outbreak in the capital of Brazil, Brasilia, under several scenarios of mobility restriction. We show that the distribution of epidemic outcomes can be divided into short-lived mild outbreaks and longer severe ones. We demonstrate that quarantines have the effect of reducing the probability of a severe outbreak taking place but are unable to mitigate the magnitude of these outbreaks once they happen. Finally, we present the probability of a particular trajectory in the epidemic progression resulting in a massive outbreak as a function of the cumulative number of cases at the end of each quarantine period, allowing for the estimation of the risk associated with relaxing mobility restrictions at a given time.

I. INTRODUCTION

With the worldwide diffusion of the severe acute respiratory syndrome coronavirus 2 (SARS-CoV-2) [1,2], researchers across many fields, such as physics [3–5], pharmacology [6,7], and biology [8,9], are contributing in the fight against the pandemic. One particular area of interest is the modeling of the evolution of the coronavirus disease 2019 (COVID-19) outbreak in different parts of the world to guide policymakers and gauge the efficacy of proposed interventions.

As a first approach to epidemic modeling, phenomenological models provide a simple analytical expression calibrated by the available data to model important epidemiological variables and provide short-term forecasts of the epidemic's progression [10]. Such models include generalized growth models, suitable for the initial stages of the epidemic, or logistic models as the Richards growth model (RGM) [11], which are more appropriate for later stages [3,12]. However, when it comes to analyzing the effects of different interventions in the development of an epidemic, the phenomenological models are not able, by themselves, to provide the connection between the intervention and model parameters. Approaches with additional complexity are required in such cases. In this sense, agent-based models, which simulate the interactions between people, allow the evaluation of mitigation strategies in the early stages of the epidemic, guiding measures of health and political authorities [13,14].

Generally, epidemiological models rely on the population's compartmentalization in categories whose occupation varies in time [15,16]. An example is the SEIR model, in which individuals in a population are considered susceptible (S), exposed (E), infectious (I), or recovered (R). Whereas susceptible individuals are those who are not immune to the disease, "exposed" refers to those to whom the virus has been transmitted but are not yet able to infect others. The capacity to transmit the virus characterizes infectious individuals. Finally, after the infectious individuals are either cured or die from the disease, they are considered to belong to the recovered category, at which point they no longer can be infected. In deterministic models, the number of individuals in each category is often governed by a set of differential equations, which are solved to yield the time dependence of each category's occupation number, allowing, in principle, for making forecasts regarding the evolution of the outbreak.

However, deterministic models do not take into account the random aspects that, especially in the case of complex environments such as those that involve the transmission of a virus in a city, may significantly impact the outcomes, rendering deterministic predictions meaningless. In this sense, stochastic epidemic models have been developed [17–21] including models that rely, for instance, on Markov chains or stochastic differential equations to arrive at a distribution of outcomes that may result from a given set of initial conditions.
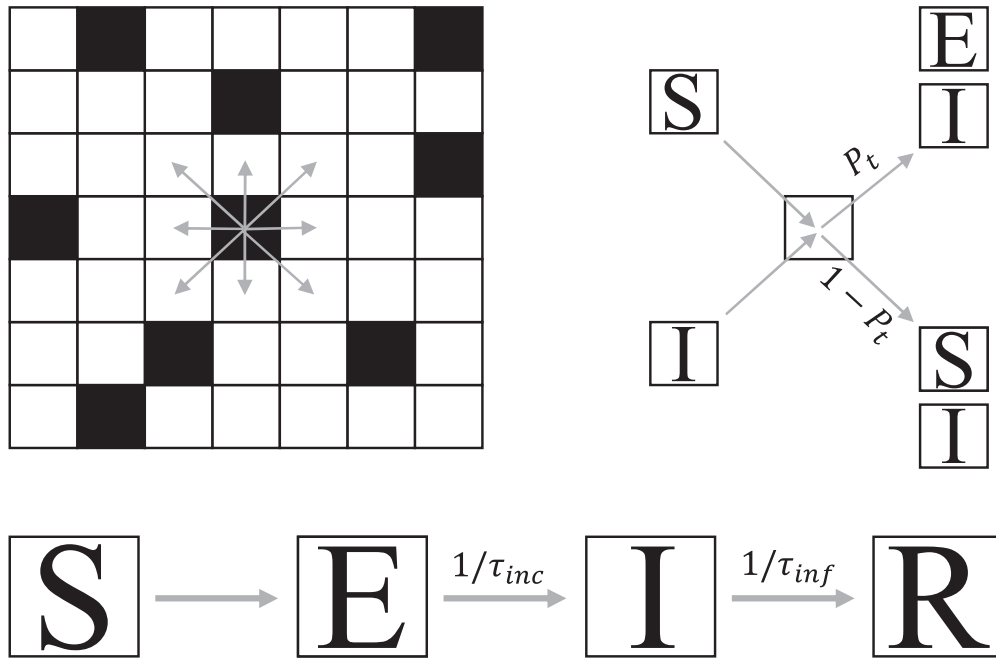
[*]dasf@unb.br

FIG. 1. Schematics of the KMC model. Individuals (black squares) are able to move in a grid by jumping to nearby sites. When a susceptible (S) individual and an infected (I) one meet, the susceptible may become exposed (E) with probability p_t. Exposed individuals turn infectious with a rate of $1/\tau_{\rm inc}$ and infectious individuals are removed (either cured or dead) with rate $1/\tau_{\rm inf}$.

This allows one to obtain answers to questions regarding the duration and severity of an outbreak in probabilistic terms.

We have developed a kinetic Monte Carlo (KMC) implementation of an age-structured SEIR model in this work. This new stochastic model is inspired by similar simulations that have been successfully employed in materials science [22,23]. It focuses on the mobility of individuals and demography as critical aspects in determining possible outcomes for an outbreak. The model is used to study the effect of mobility restriction on the evolution of a COVID-19 outbreak. By selecting model parameters to reflect the characteristics of the city of Brasilia, Brazil, we were able to present a distribution of possible outcomes under scenarios in which mobility restriction measures were imposed for different time periods. We determine that the probability of occurrence of large outbreaks is affected by quarantine duration, but this measure is unable to decrease the severity of a massive outbreak when it takes place. Finally, we present the probabilities for different outcomes in each scenario and provide a means to gauge the likelihood of success of lifting mobility restrictions as a function of the cumulative number of infected individuals.

II. METHODS

A. The KMC model

The model is set on a $N \times N$ two-dimensional square lattice in which sites are set apart by a distance d from each other in the vertical and horizontal directions. The lattice spans a specific area that is populated by several individuals. This number is chosen in such a way as to reproduce a particular urban density ($\rho_{\rm urb}$). Each individual is randomly assigned an age with a probability distribution corresponding to the region's age pyramid. Finally, the individuals are placed

randomly on the grid, and periodic boundary conditions are enforced to prevent border effects. An initial fraction ρ_0 of the individuals is assumed to be infectious, whereas the rest of the population is considered susceptible to the infection.

After the model is populated, the simulation starts. Each individual is able to move by stepping toward one of their eight nearest-neighboring cells (four in the vertical and horizontal directions and four in the diagonal directions), as shown in Fig. 1. The rate with which a move between two sites takes place is given by

$$k_s = \frac{1}{\tau}\left(\frac{L}{r}\right),\qquad(1)$$

in which τ is the time unit, r is the intersite distance, and L is a measure of the individual's mobility. Setting τ to 1 day allows us to interpret the ratio L/r as the number of steps an individual takes in a day. Accordingly, L becomes the average distance covered by an individual in a day.

The actual site to which an individual in the simulation moves is determined by calculating the step rates to each of its eight neighboring sites. The probability of each site (identified by $i = 1, 2, \ldots, 8$) being chosen is given by

$$p_i = \frac{k_{\rm si}}{\sum_i k_{\rm si}},\qquad(2)$$

in which $k_{\rm si}$ corresponds to the jumping rates to each neighboring site.

At this point, a random number is drawn to select the site that may receive the individual. This process of outcome selection is repeated for every person in the simulation. As a result, a transfer rate k_j is associated to each individual corresponding to the selected movement. The inverse of the largest such rate among all individuals ($k_{\rm max}$) corresponds to the time

step of the simulation. The ratio between each moving rate and the maximum one ($k_j/k_{\max}$) is used as the probability of each individual's selected movement being allowed at that particular simulation step. This way, the higher a person's mobility (larger moving rates), the higher the probability of moving at each step.

The moving process competes against two other processes in the case of infectious individuals: Death and recovery. These latter processes occur with rates k_d and k_r, respectively. The death rate is calculated as $\mathrm{IFR}/\tau_{\inf}$, where $\tau_{\inf}$ is the average duration of the infectious period, and IFR is the infection fatality rate, which may vary according to the age group of the individual. Likewise, the recovery rate is given by $(1 - \mathrm{IFR})/\tau_{\inf}$. As such, once a site is chosen for moving, a second random number is drawn to determine whether the infected individual moves, dies, or recovers from the disease. Again, each outcome has probability given by the process rate divided by $(k_s + k_d + k_r)$. If a subject dies or recovers, then they are removed from the simulation. In this manner, we consider recovered individuals to have become immune to further infection.

A similar measure is taken regarding exposed individuals. In this case, the competing process is their conversion to the infectious category. This conversion happens with a rate $k_c = 1/\tau_{\inc}$, in which $\tau_{\inc}$ is the mean incubation period. The conversion process has probability $k_c/(k_c + k_s)$, and if it is selected, then the individual becomes infectious. We consider that all exposed individuals eventually become infectious [27]. This mechanism for conversion between exposed to infectious and from infectious to removed results in exponentially distributed incubation and infectious periods [22,23].

After this step is concluded and all individuals have either moved, stayed put, or been removed from the simulation, we check whether there is any site at which an infectious and a susceptible individuals have met. If so, then the susceptible individual turns exposed with a transmission probability p_t (as shown in Fig. 1). The time, location, and age of individuals that die, recover, or become exposed or infectious are registered. After that, the whole process is repeated until no infectious or exposed individuals remain in the simulation. A large number of rounds are run so that statistical analysis of the results is possible.

B. Determining model parameters

The characteristic infection and incubation periods employed in the simulations, as well as the transmission probability per contact associated with the virus, are shown in Table I, following recent research on the subject.

TABLE I. Parameters concerning the behavior of COVID-19 employed in the simulations

Parameter	Value	Reference
Avg. incubation period ($\tau_{\inc}$)	6.4 days	[24,25]
Avg. infectious period ($\tau_{\inf}$)	7 days	[25,26]
Transmission probability (p_t)	0.10–0.30 per contact	Assumed

TABLE II. Brasilia's population, IFR, and relative mobility for several age groups according to Refs. [13,28,29].

Age	Population (%) [28]	IFR (%) [13]	Relative mobility [29]
0–9	15.1	0.002	0.50
10–19	17.1	0.006	0.85
20–29	20.1	0.03	0.91
30–39	18.1	0.08	0.84
40–49	13.5	0.15	0.81
50–59	8.5	0.6	0.78
60–69	4.5	2.2	0.72
70–79	2.2	5.1	0.60
80+	0.9	9.3	0.60

Next, in order for simulations to reflect the behavior of transmission in a given city, it is necessary to adjust the model parameters accordingly. The first parameter in this sense is the urban density ρ_{urb}, which is information that is readily available for most cities and corresponds to 4729 people/km^2 in the case of Brasilia [28]. We choose the number of individuals in the simulation so that the lattice's average population density matches this value. Also important is the age distribution of the population, as it is known that age is a significant factor in mortality rates [13] and is associated with varying degrees of mobility [29]. Table II presents the age pyramid for the city of Brasilia as well as the IFR of COVID-19 for each age group.

Mobility in this model is expressed in terms of the average daily number of steps taken by an individual. We write this number as $S = S_0 M$, where S_0 is a baseline number of steps, and M is the relative mobility, which is a function of age group and is also presented in Table II. The average number of steps observed for each age group under normal conditions is reproduced with $S_0 = 6000$ steps per day (spd) [29]. We model quarantine conditions by reducing this S_0 term to 2000 spd, corresponding to a 66% decrease in overall mobility in the population.

Finally, lattice size N and intersite distance d determine the surface area of the simulation. Ideally, one could choose d as small as an average step size, say, 0.5 m, but that would require a huge lattice for a reasonable population to be simulated. For this reason, a scheme is required to perform the simulations with much larger intersite distances without modifying the results. The key is choosing the parameters in such a way as to produce the same diffusion constant for the population.

For jumping rates of L/d jumps per day, the diffusion constant can be shown to correspond to Ld m^2/day. Considering a person takes an average number S of steps per day with an average length of $d = 0.5$ m results in a daily covered distance $L = 0.5S$ and a diffusion constant of $(0.5^2)S$ m^2/day. As such, for a given daily number of steps, an equivalent coarse-grained simulation can be performed by choosing more suitable values of d and L such that:

$$Ld = (0.5^2)S. \qquad (3)$$

For the simulation shown here, a 50×50 lattice was employed, the intersite distance d was set to 20 m, resulting in $L = 75$ m and $L = 25$ m under regular and quarantine con-
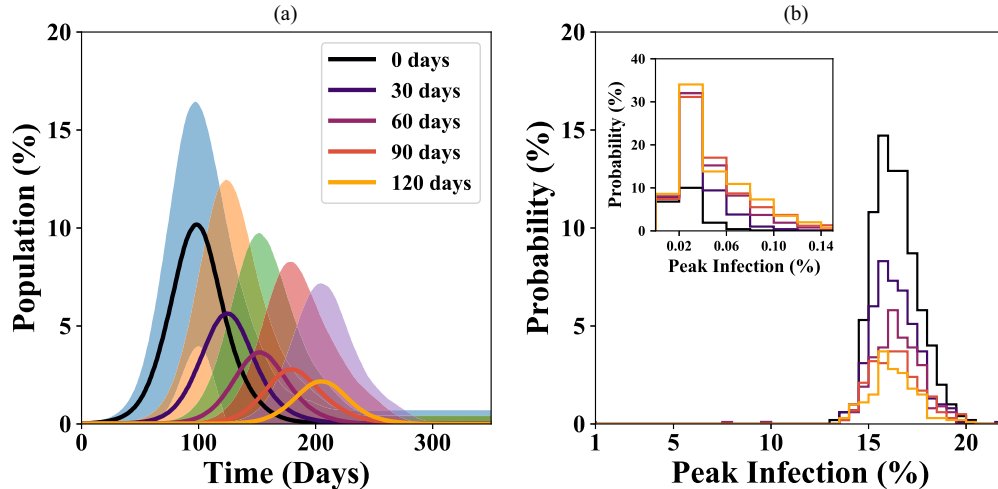
FIG. 2. (a) Average number of active infectious individuals as a function of time for different quarantine scenarios and $p_t = 0.30$. The shaded area corresponds to one standard deviation. (b) Histograms showing the distribution of peaks of the infection curves in the $p_t = 0.30$ case. The inset shows in details the distribution in the 0.02% to 0.15% population range.

ditions, respectively. Simulations for each analyzed scenario were run 1000 times.

III. RESULTS AND DISCUSSION

To analyze the effects of enforcing a reduction in overall mobility for different periods, we ran simulations for scenarios in which these restrictions are applied for a number of days that ranges from 0, that is, no intervention at all, to 120 days. Once these time limits are reached, the regular mobility regime is reintroduced. In each scenario, a fraction of 0.02% of the total population was considered infectious at the initial moment of the simulation. In the case of Brasilia, with its approximately three million people population, this would amount to roughly 600 simultaneously active infectious individuals.

The main concern regarding the fast propagation of the COVID-19 virus lies in the possible pressure on each city's healthcare system due to the large number of infected people requiring hospitalization at the same time. As such, we start looking into the simulation results by analyzing the evolution of the total number of active infectious individuals as a function of time. Figure 2(a) shows results averaged from the 1000 simulations run with $p_t = 0.30$ in each scenario with shaded areas corresponding to one standard deviation intervals. This metric leads to the belief that mobility restriction results in both a progressive decrease and delay of the curve's peak, a phenomenon that has been dubbed the "flattening of the curve."

However, analyses made in terms of average results are deceiving. It can be seen that the uncertainty in the results is large, which prompts an investigation into the behavior of the distribution of curves from individual simulations as well. In this sense, Fig. 2(b) shows the histograms corresponding to the distribution of the peak values of the infection curves in the $p_t = 0.30$ case. The distribution is bimodal, with the number of simultaneously infected individuals in the population peaking at values below 1% in some simulations and between 15%

and 20% in others. Interestingly, this is the case even for the simulations with no mobility restriction, which present a 20% chance of developing only a mild outbreak regardless of the lack of transmission mitigation measures.

We also observe that the effect of the mobility restriction lies in the shifting of the number of simulations that belong to each peak, with longer quarantines being associated with larger probabilities of peak infection number remaining below 1%. The inset of Fig. 2(b) shows in detail the distribution of peak values in the 0.02% to 0.15% population interval. Nearly 8% of the simulations are found to produce infection peaks at the 0.02% mark, which coincides with the initial proportion of the population that was considered to be infected. As such, these simulations correspond to cases in which the virus fails to spread. The most common result in this initial range, on the other hand, is seen to be a peak of 0.04% of the population. Peaks amounting to more significant fractions of the population are also observed with probabilities that decrease accordingly until practically vanishing at the 0.15% mark. These cases constitute the best-case scenarios for the outbreak's evolution, meaning short-lived outbreaks that affect only a small portion of the population. Such was the case, for instance, of the SARS outbreak in 2002–2003, which had a short duration and resulted in a relatively low number of cases [30].

Interestingly, we note that mobility restriction, regardless of its duration, does not reduce the infection curve's peak. This is evidenced by the fact that for all scenarios, both the leftmost and rightmost peaks in Fig. 2(b) are located near the same values, although with different probabilities of being reached. In this sense, the progressive "flattening of the curve" becomes, in this model, a mere artifact of averaging over this bimodal distribution. The actual effect of imposing mobility restrictions becomes only the reduction in the probability of large-scale outbreaks.

The same conclusions apply to simulations run with transmission probabilities (p_t) of 0.20 and 0.15, which have their peak infection curves shown in Fig. 1 in the Supplemental Material [31]. The effect of reducing this probability is twofold.
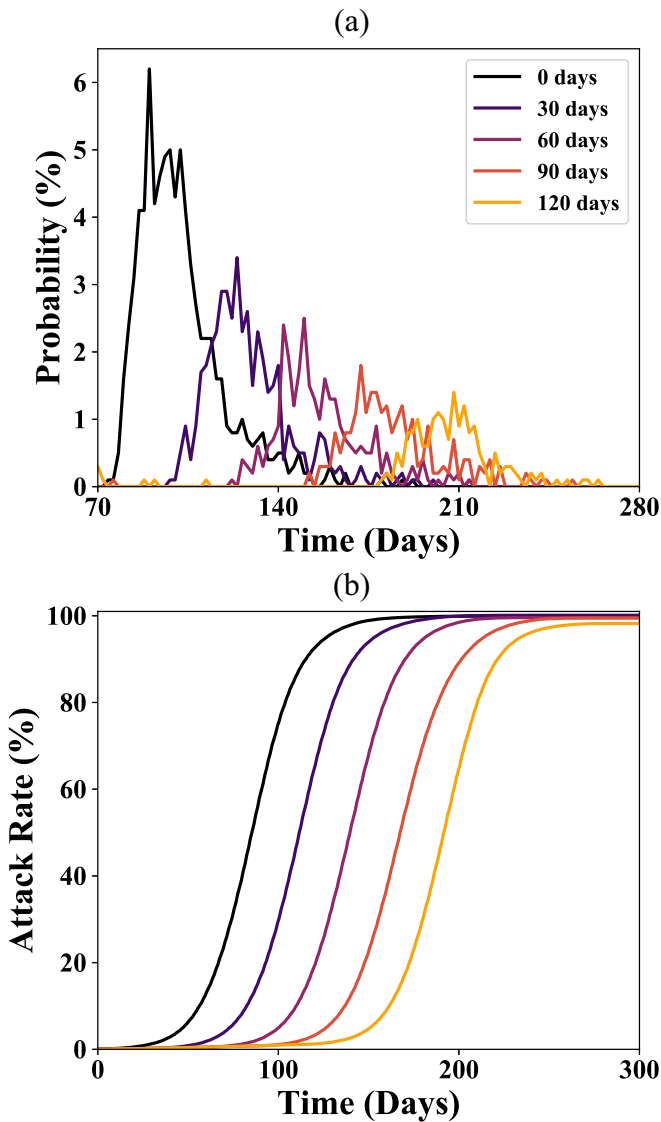
FIG. 3. (a) Distribution of the number of days for peaks in the infection curves to be reached in the case of simulations that resulted in large outbreaks. (b) Average attack rate taken from simulations that produced large outbreaks as a function of time for the different mobility restriction scenarios.

First, it increases the chance of outbreaks being mild. Second, it reduces the maximum amount of simultaneously infectious individuals to between 10–15% and 5–10% in the $p_t = 0.20$ and $p_t = 0.15$ cases, respectively. It is worth noting that for $p_t = 0.10$ large outbreaks become rare regardless of mobility restriction.

If the reduction in peak value is not observed in the simulations with different mobility restrictions, on the other hand, then a delay in the appearance of the peaks is seen. Focusing only on the large outbreaks, Fig. 3(a) shows the distribution of the number of days for the peak of the infection curve to take place in the $p_t = 0.30$ case. There is a clear progression showing that longer periods of restricted mobility translate into a delay in the number of days for peaks to be reached, as expected. When no mobility restriction is applied, the peak in the number of infectious individu-

als happens most likely 90 days after the beginning of the simulations. This number is increased in the exact amount of the quarantine duration for each other scenario shown in Fig. 3(a), amounting effectively to a time shift in the simulations.

We now turn our attention to the attack rate of the virus, that is, the proportion of the population that gets infected during the course of the simulation and its behavior under the different mobility restriction scenarios. In this sense, Fig. 3(b) presents the average attack rate as a function of time for all quarantine durations in the $p_t = 0.30$ case. These averages are taken only from simulations for which at least 1% of the population has been infected by the 600th day. These simulations correspond to those that present larger and delayed peaks in the infection curve, as seen in Figs. 2(b) and 3(a), as opposed to the simulations for which the virus fails to spread significantly. It can be seen that in all cases the average attack rate approaches 100% before the 300th day. The different mobility restriction regimes are seen to delay the spread of the virus by extending the periods of slow growth in the number of cases. However, after regular mobility is restored, contagion accelerates drastically. These results are in line with those of Fig. 2(b) and again show that, under model conditions, mobility restriction does not significantly affect the size of the epidemic once contagion reaches over 1% of the population. For transmission probabilities $p_t = 0.20$, final average attack rates are the same as the ones in Fig. 3(b). When the contagion probability is decreased to 0.15, then average attack rates drop, for instance, to 84% in the no quarantine case. In both cases, as can be seen in Fig. 2 in the Supplemental Material [31], we observe that at the 300th day attack rates are lower than what is seen in the $p_t = 0.30$ case, which shows that the reduction in the chance of contagion delays the progression of the epidemic, as expected.

In addition to the behavior of the infection curves, the evolution of the outbreak may also be analyzed by looking into the behavior of the reproduction number R, that is, the average number of people to whom an infected person transmits the virus during its infectious period. The average reproduction number, considering only simulations in which the virus is still active after quarantine, is shown in Fig. 4(a) as a function of time for the $p_t = 0.30$ case. The initial time is taken as the seventh day after the mobility restrictions are relaxed so as to allow for a better comparison between different scenarios. It can be seen that for the no quarantine simulations, a basic reproduction number of 4.3 is reached. This number drops in the following days, becoming equal to what is observed in the other scenarios. Interestingly, all scenarios that included mobility restrictions present very similar behavior concerning the average reproduction number of the remaining active simulations, with an initial value of around 2.2. It is worth noting that such a number is close to previously reported values for COVID-19 [13,32]. In each case, it is only around 50 days after quarantine is over that these still active outbreaks display a reduction in their reproduction number.

The above results again reinforce the observation that even though mobility restriction measures may reduce the probability of a severe outbreak, they are unable, under model conditions, to change the characteristics of these severe outbreaks. In fact, considering again Fig. 4(a), we may think of
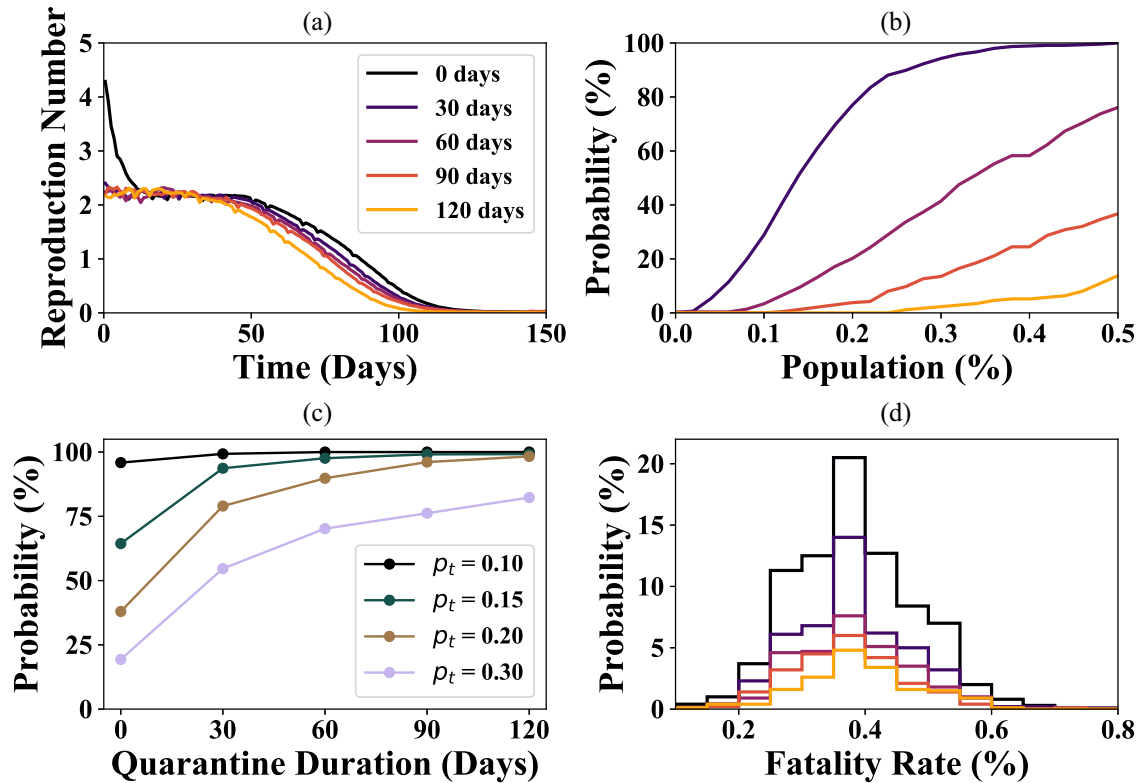
FIG. 4. (a) Average reproduction number as a function of time for simulations with still active infections after quarantine. Time starts counting from the seventh day after the end of quarantine in each scenario. (b) Cumulative conditional probability of an outbreak resulting in >90% infected individuals as a function of the cumulative number of cases at the end of quarantine. (c) Probability of at most 1% of the population being infected as a function of quarantine duration. (d) Distribution of the total number of deaths for simulations with different periods of quarantine.

the time at which mobility restriction ends as constituting the initial time of simulations that are run with different initial conditions but that produce nearly the same progression. Furthermore, tests with simulations run with more strict mobility restrictions ($S_0 = 1200$ spd) that ended up in large outbreaks showed the same behavior as of the simulations presented here. These results indicate that the characteristics of large outbreaks are determined by the combination of mobility, demography, and transmission probability rather than from the initial conditions of the simulations. A similar insensitivity to initial conditions was observed in the context of an irreversible epidemic model that showed that the location of an initial spreader in a network affects the probability of outbreaks but not their average magnitudes [33].

The existence of simulations that present large reproduction numbers even after the quarantine ends prompts the question of what is the likelihood that, given one particular realization of the process, the situation will deteriorate to the more acute scenarios, that is, those corresponding to the rightmost peaks observed in Fig. 2(b) with more than 90% of the population being infected. The answer is given in Fig. 4(b), which shows the cumulative conditional probability of the outbreak becoming uncontrolled, given the cumulative number of cases registered at the end of each quarantine scenario. We see that for a 30-day quarantine, if the number of infections reaches up to 0.1% of the total population (around 3000 people in the case of Brasilia), then there is a 28% probability of the outbreak affecting the entire population. This number

drops to 4% in the case of a 60-day quarantine and 0% for longer ones.

It is noteworthy how the probabilities of Fig. 4(b) increase so sharply in the interval from 0 to 0.5%. This goes to show the importance of acting quickly in the face of an outbreak, since if the cumulative number of infected individuals reaches 1% of the population, then even the 120 days quarantine has less than 50% chance of keeping the outbreak under control.

In this sense, we may obtain the probabilities of an outbreak ending up infecting at most 1% of the population as a function of quarantine duration. These are shown in Fig. 4(c) for different transmission probability values. We see that with no intervention there is a 20% chance of the outbreak remaining limited in the $p_t = 0.30$ case. This number increases to 54% for a 30-day quarantine and 70% for 60 days. From 90 to 120 days, the increase in probability is of only 4%, from 78% to 82%. The apparent saturation in the probabilities is indicative that total elimination of the risk of widespread diffusion of the disease is not possible for the urban density, mobility, and transmission probability employed in these simulations. Importantly, the situation improves significantly if the probability of contagion is reduced. For $p_t = 0.15$, for instance, the 30-day quarantine is enough to make the probability of a mild outbreak to reach 94%. In addition, the payoffs in reducing p_t are nonlinear, which indicates that the early adoption of measures that diminish even slightly the probability of contagion per contact, such as the use of face masks, may prove mostly beneficial.

Finally, we take a look at the distribution of the total number of fatalities in the different quarantine scenarios. These can be seen in Fig. 4(d) for the $p_t = 0.30$ case, which focuses on the fatality rates as a fraction of the city's population associated with the larger outbreaks. Whereas the simulations for which the outbreak is contained present near-zero additional deaths, that is, not counting the ones that may have happened until the initial conditions of the simulations were achieved, the more severe outbreaks show a total death toll ranging from 0.2% to 0.6% of the population. The distribution peak is again the same for all quarantine scenarios, with longer periods of restricted mobility decreasing the likelihood of the most acute outcomes taking place. Importantly, these estimates do not take into account second-order effects that may modify the IFR, such as the collapse of the city's healthcare system. Even disregarding such second-order effects, we see that avoidance of the worst-case scenarios could result in the prevention of around 10 000 deaths considering Brasilia's roughly 3 million population and the IFR estimates used here. For lower transmission probabilities ($p_t = 0.15$ and 0.20), the chances of such large fatality rates decrease but, as shown in Fig. 3 in the Supplemental Material [31], the shape of the fatality distribution remains the same.

It is important to stress that even though the model presented here may be useful to understand how well mobility restrictions influence the epidemic outbreak, the predictive power of the model, meaning its capacity to indicate how the epidemic will actually progress in the city, is limited, as it does not take into account, for instance, the possibility of new infections being seeded by people coming from other cities, which could restart an epidemic. It also does not account for the variability in how populations either comply or disregard the mobility restriction orders that have also themselves been subject to modifications during the course of the epidemic. In this sense, the model serves the purpose of indicating possible scenarios and gauge the efficiency of proposed measures. However, the KMC simulations shown here can be easily modified to include several different factors that may be deemed important in further research.

IV. CONCLUSIONS

In summary, we have developed a stochastic epidemic model based on kinetic Monte Carlo simulations. The model focuses on the interplay between demography and age-structured mobility data to study the evolution of the COVID-19 disease outbreak in Brasilia, Brazil, under different quarantine scenarios. Results show that outcomes can be divided into two groups for simulations with a transmission probability of 0.30. The first one consists of short-lived outbreaks that present attack rates limited to less than 0.5% of the population, constituting cases in which the virus fails to spread. The second group, on the other hand, is composed of simulations with more than 90% attack rate and longer durations, taking around 90 days after mobility restrictions are relaxed to reach a peak in the number of simultaneously infectious individuals. This peak ranges from 15% to 20% of the population and may result in a 0.4–0.6% death rate according to the available IFR estimates.

If transmission probabilities are reduced, then a comparable decrease in the peak of simultaneously infectious individuals is observed as well as an increase in the probability of outbreaks being contained. However, for larger outbreaks, the reduced chance of contagion increases the amount of time it takes for the spreading to conclude and reduces the average attack rate slightly. Overall, the behavior of the simulations remains qualitatively the same for p_t in the range 0.15–0.30. For a p_t of 0.10, on the other hand, we practically do not observe major outbreaks taking place.

Interestingly, we observe that quarantine, modeled as a mobility decrease in the whole population, has the effect of reducing the probability of occurrence of large outbreaks, with longer duration being associated with a higher chance of the virus failing to spread. More importantly, we show that quarantine duration is not able to affect the magnitude of an outbreak once the virus is able to infect 1% of the population. This is true even for simulations performed with lower transmission probabilities.

Finally, we have provided estimates for the probability of a particular trajectory belonging to the more severe outcome group as a function of the cumulative number of cases at the end of each quarantine period. These results are particularly important as they could provide guidance when it comes to deciding how risky it is to relax mobility restriction measures, a decision that has to be made eventually.

[1] Q. Li, X. Guan, P. Wu, X. Wang, L. Zhou, Y. Tong, R. Ren, K. S. Leung, E. H. Lau, J. Y. Wong *et al.*, Early transmission dynamics in Wuhan, China, of novel coronavirus–infected pneumonia, New Engl. J. Med. **382**, 1199 (2020).

[2] N. Zhu, D. Zhang, W. Wang, X. Li, B. Yang, J. Song, X. Zhao, B. Huang, W. Shi, R. Lu *et al.*, A novel coronavirus from patients with pneumonia in China, 2019, New Engl. J. Med. **382**, 727 (2020).

[3] G. L. Vasconcelos, A. M. Macêdo, R. Ospina, F. A. Almeida, G. C. Duarte-Filho, and I. C. Souza, Modelling fatality curves of COVID-19 and the effectiveness of intervention strategies, PeerJ **8**, e9421 (2020).

[4] J. Schuttler, R. Schlickeiser, F. Schlickeiser, and M. Kroger, COVID-19 predictions using a Gauss model, based on data from April 2, medRxiv (2020).

[5] I. Ciufolini and A. Paolozzi, Mathematical prediction of the time evolution of the COVID-19 pandemic in Italy by a Gauss error function and Monte Carlo simulations, Eur. Phys. J. Plus **135**, 355 (2020).

[6] J. Gao, Z. Tian, and X. Yang, Breakthrough: Chloroquine phosphate has shown apparent efficacy in treatment of COVID-19 associated pneumonia in clinical studies, Biosci. Trends **14**, 72 (2020).

[7] S. Pant, M. Singh, V. Ravichandiran, U. Murty, and H. K. Srivastava, Peptide-like and small-molecule inhibitors against COVID-19, J. Biomol. Struct. Dyn., 1 (2020).

[8] E. Dong, H. Du, and L. Gardner, An interactive web-based dashboard to track COVID-19 in teal time, Lancet Infect. Dis. **20**, 533 (2020).

[9] A. D. Elmezayen, A. Al-Obaidi, A. T. Şahin, and K. Yelekçi, Drug repurposing for coronavirus (COVID-19): in silico screening of known drugs against coronavirus 3CL hydrolase and protease enzymes, J. Biomol. Struct. Dyn., 1 (2020).

[10] G. Chowell, D. Hincapie-Palacio, J. Ospina, B. Pell, A. Tariq, S. Dahal, S. Moghadas, A. Smirnova, L. Simonsen, and C. Viboud, Using phenomenological models to characterize transmissibility and forecast patterns and final burden of Zika epidemics, PLoS Curr. **8** (2016).

[11] F. Richards, A flexible growth function for empirical use, J. Exp. Bot. **10**, 290 (1959).

[12] K. Wu, D. Darcet, Q. Wang, and D. Sornette, Generalized logistic growth modeling of the COVID-19 outbreak in 29 provinces in China and in the rest of the world, Nonlinear Dyn., 1 (2020).

[13] N. Ferguson, D. Laydon, G. Nedjati Gilani, N. Imai, K. Ainslie, M. Baguelin, S. Bhatia, A. Boonyasiri, Z. Cucunuba Perez, G. Cuomo-Dannenburg, A. Dighe, I. Dorigatti, H. Fu, K. Gaythorpe, W. Green, A. Hamlet, W. Hinsley, L. Okell, S. Van Elsland, H. Thompson, R. Verity, E. Volz, H. Wang, Y. Wang, P. Walker, C. Walters, P. Winskill, C. Whittaker, C. Donnelly, S. Riley, and A. Ghani, Impact of non-pharmaceutical interventions (NPIs) to reduce COVID-19 mortality and healthcare demand, Imperial College London, 1 (2020).

[14] J. R. Koo, A. R. Cook, M. Park, Y. Sun, H. Sun, J. T. Lim, C. Tam, and B. L. Dickens, Interventions to Mitigate early spread of SARS-CoV-2 in Singapore: A modelling study, Lancet 12 Infect. Dis. **20**, 678 (2020).

[15] R. M. Anderson, B. Anderson, and R. M. May, *Infectious Diseases of Humans: Dynamics and Control* (Oxford University Press, Oxford, 1992).

[16] O. Diekmann and J. A. P. Heesterbeek, *Mathematical Epidemiology of Infectious Diseases: Model Building, Analysis and Interpretation* (John Wiley & Sons, New York, 2000), Vol. 5.

[17] N. T. Bailey *et al.*, *The Mathematical Theory of Infectious Diseases and Its Applications* (Charles Griffin & Company Ltd, Bucks, UK, 1975).

[18] L. J. Allen, An introduction to stochastic epidemic models, in *Mathematical Epidemiology* (Springer, Berlin, 2008), pp. 81–130.

[19] T. Britton, Stochastic epidemic models: A survey, Math. Biosci. **225**, 24 (2010).

[20] H. Andersson and T. Britton, *Stochastic Epidemic Models and Their Statistical Analysis* (Springer Science & Business Media, New York, 2012), Vol. 151.

[21] L. J. Allen, A primer on stochastic epidemic models: Formulation, numerical simulation, and analysis, Infect. Dis. Model. **2**, 128 (2017).

[22] L. E. de Sousa, D. A. da Silva Filho, R. T. de Sousa, and P. H. de Oliveira Neto, Exciton diffusion in organic nanofibers: A Monte Carlo Study on the effects of temperature and dimensionality, Sci. Rep. **8**, 1 (2018).

[23] L. E. de Sousa, P. H. de Oliveira Neto, J. Kjelstrup-Hansen, and D. A. da Silva Filho, Modeling temperature dependent singlet exciton dynamics in multilayered organic nanofibers, J. Chem. Phys. **148**, 204101 (2018).

[24] J. A. Backer, D. Klinkenberg, and J. Wallinga, Incubation period of 2019 novel noronavirus (2019-nCoV) infections among travellers from Wuhan, China, 20–28 January 2020, Eurosurveillance **25**, 2000062 (2020).

[25] K. Prem, Y. Liu, T. W. Russell, A. J. Kucharski, R. M. Eggo, N. Davies, S. Flasche, S. Clifford, C. A. Pearson, J. D. Munday *et al.*, The effect of control strategies to reduce social mixing on outcomes of the COVID-19 epidemic in Wuhan, China: A modelling study, Lancet Publ. Health **5**, e261 (2020).

[26] R. Woelfel, V. M. Corman, W. Guggemos, M. Seilmaier, S. Zange, M. A. Mueller, D. Niemeyer, P. Vollmar, C. Rothe, M. Hoelscher *et al.*, Clinical presentation and virological assessment of hospitalized cases of coronavirus disease 2019 in a travel-associated transmission cluster, MedRxiv (2020).

[27] D. P. Oran and E. J. Topol, Prevalence of asymptomatic SARS-CoV-2 infection, Ann. Intern. Med. **173**, 362 (2020).

[28] Brasilia's urban density data, provided by the governmental agency CODEPLAN (Planning Company of the Federal District), publicaly available on the web at: http://infodf.codeplan.df.gov.br/?page_id=278 (2020).

[29] T. Althoff, J. L. Hicks, A. C. King, S. L. Delp, J. Leskovec *et al.*, Large-scale physical activity data reveal worldwide activity inequality, Nature (London) **547**, 336 (2017).

[30] S. Riley, C. Fraser, C. A. Donnelly, A. C. Ghani, L. J. Abu-Raddad, A. J. Hedley, G. M. Leung, L.-M. Ho, T.-H. Lam, T. Q. Thach *et al.*, Transmission dynamics of the etiological agent of SARS in Hong Kong: Impact of public health interventions, Science **300**, 1961 (2003).

[31] See Supplemental Material at http://link.aps.org/supplemental/10.1103/PhysRevE.102.032133 for peak infection curves, average attack rates, and distribution of total number of fatalities in simulations for $p_t = 0.20$ and 0.30.

[32] A. J. Kucharski, T. W. Russell, C. Diamond, Y. Liu, J. Edmunds, S. Funk, R. M. Eggo, F. Sun, M. Jit, J. D. Munday *et al.*, Early dynamics of transmission and control of COVID-19: A mathematical modelling study, Lancet Infect. Dis. **20**, 553 (2020).

[33] B. Min, Identifying an influential spreader from a single seed in complex networks via a message-passing approach, Eur. Phys. J. B **91**, 18 (2018).